ELSEVIER

Engineering Analysis with Boundary Elements 30 (2006) 925–939

ENGINEERING ANALYSIS with BOUNDARY ELEMENTS

www.elsevier.com/locate/enganabound

A Lagrangian approach for quantum-mechanical electrostatic analysis of deformable silicon nanostructures

G. Li, N.R. Aluru*

Department of Mechanical Science and Engineering, Beckman Institute for Advanced Science and Technology, University of Illinois at Urbana-Champaign, Urbana, IL 61801, USA

Received 7 January 2006; accepted 12 March 2006
Available online 18 September 2006

Abstract

Semiconductor mechanical components of nanoelectromechanical systems (NEMS) typically undergo deformations when subjected to electrostatic forces. Computational analysis of electrostatic NEMS requires an electrostatic analysis to compute the electrostatic forces acting on the nanomechanical structures and a mechanical analysis to compute the deformation of the nanomechanical structures. Typically, the mechanical analysis is performed by a Lagrangian approach using the undeformed position of the structures. However, the electrostatic analysis is performed by using the deformed position of the nanostructures. The electrostatic analysis on the deformed position of the nanostructures requires updating the geometry of the structures during each iteration. In this paper, based on a recently proposed hybrid BIE/Poisson/Schrödinger approach, we propose Lagrangian formulations for the BIE/Poisson/Schrödinger equations and solve the coupled Lagrangian BIE/Poisson/Schrödinger's equations self-consistently using the undeformed position of the semiconductors to compute the charge distributions on the deformed semiconductors. The proposed approach eliminates the requirement of updating the geometry and, consequently, significantly simplifies the procedure of coupled electromechanical analysis of NEMS.

Keywords: Lagrangian electrostatics; Quantum-mechanical electrostatic analysis; Nanoelectromechanical systems (NEMS)

1. Introduction

A number of nanoelectromechanical device and system (NEMS) applications have been proposed recently [1–3]. Computational analysis of electrostatically actuated NEMS requires a self-consistent analysis of the coupled electrostatic and mechanical energy domains [4]. Typically, a NEM system contains a deformable and a fixed structure separated by a dielectric medium. The deformable structure is typically made of a semiconductor material, such as silicon, and the fixed structure can be either a conductor or a semiconductor. When a voltage is applied between the deformable and the fixed structures, electrostatic forces act on both the structures due to the induced charges. Since the fixed structure cannot move, the electrostatic forces move only the deformable structure. When the deformable semiconductor structure undergoes a shape change, the charge redistributes in the structure and, consequently, the resultant electrostatic forces and the deformation of the structure also change. This process continues until an equilibrium state is reached. The primary steps involved in the self-consistent solution approach are summarized in Algorithm 1.

Algorithm 1. Procedure for coupled electromechanical analysis

repeat
1. Do mechanical analysis (on the undeformed geometry) to compute structural displacements
2. Update the geometry of the semiconductor using the computed displacements
3. Compute charge distribution in the semiconductor by electrostatic analysis (on the deformed geometry)
4. Compute electrostatic forces (on the deformed geometry)

*Corresponding author.
E-mail address: aluru@uiuc.edu (N.R. Aluru).
URL: http://www.uiuc.edu/~aluru.

0955-7997/$ - see front matter © 2006 Elsevier Ltd. All rights reserved.
doi:10.1016/j.enganabound.2006.03.012

5. Transform electrostatic forces to the original undeformed configuration
until an equilibrium state is reached

In microelectromechanical systems (MEMS), the mechanical components are typically treated as conductors [5–9] and the electrostatic analysis of MEMS can be performed by solving the potential or the Laplace equation in the domain exterior to all the conductors. However, as the characteristic length in NEM structures can be comparable to the Debye length, the NEM structures can no longer be approximated as conductors. In addition, when the characteristic length of the NEM structure shrinks to several tens of nanometers, the carrier quantum confinement in the semiconductor structure [10] can impose a significant effect on the charge distribution in the mechanical components of NEMS. As a result, coupled Poisson/Schrödinger equations need to be solved self-consistently to obtain the electronic properties such as the potential field and the charge distribution of the system [11,12]. Recently, we have proposed a hybrid BIE/Poisson/Schrödinger approach for quantum-mechanical electrostatic analysis of NEMS [13].

An important aspect of NEMS is that NEM structures typically undergo deformations when subjected to electrostatic forces. The computational analysis of NEMS involves repeated mechanical and electrostatic analysis on NEM structures, as shown in Algorithm 1. The mechanical analysis is typically carried out in the undeformed configuration of the structures. However, the electrostatic analysis is typically performed on the deformed structures. Therefore, the geometry of the structures needs to be updated before an electrostatic analysis is performed during each iteration. The need to update the geometry of the structures could introduce several problems—First, flat surfaces of the structures in the initial configuration can become curved due to deformation. This requires the development of complex integration schemes on curved panels [14] to perform electrostatic analysis. Second, when the structure undergoes a very large deformation, remeshing the surface as well as the interior of the deformed structure may become necessary before an electrostatic analysis is performed. Third, interpolation functions, used in many numerical methods, need to be recomputed whenever the geometry changes. Each of these issues significantly increases the computational effort making the self-consistent analysis of electrostatic NEMS an extremely complex and challenging task. A Lagrangian approach for electrostatic analysis of deformable conductors or MEMS has been proposed and discussed in [6,8,15]. In this paper, we propose a Lagrangian formulation for the hybrid BIE/Poisson/Schrödinger equations for electrostatic analysis of deformable semiconductor nanostructures or NEMS. We refer to this approach as the Lagrangian BIE/Poisson/Schrödinger approach. The Lagrangian BIE/Poisson/Schrödinger approach eliminates the requirement of a cut-off box as well as the requirement of updating the geometry of nanostructures. While the Lagrangian approach is mathematically equivalent to the deformed configuration BIE/Poisson/Schrödinger approach, it significantly simplifies the coupled electrical and mechanical analysis procedure as shown in Algorithm 2. In addition, to take advantage of the flexibility of meshless methods (see e.g., [16]), in this paper we employ the meshless finite cloud method (FCM) [17–20] for interior analysis (i.e., for the solution of the Lagrangian Poisson/Schrödinger equations in the semiconductor) and the meshless boundary integral formulation [21–24] for exterior analysis (i.e., for the solution of the Lagrangian boundary integral equations of the exterior potential equation). The charge distribution and the capacitance of the NEMS are obtained by solving the coupled system of equations self-consistently. Since the primary focus of this paper is Lagrangian electrostatic analysis, based on quantum-mechanical models, we assume that the deformation of the nanostructure is known, i.e., we address the question of if the structure were to undergo a certain deformation, can we compute the charge density without updating the geometry (i.e., we discuss step 2 of Algorithm 2 assuming step 1 can be implemented using existing tools and techniques). For self-consistent mechanical and electrostatic analysis, the deformation can be computed by performing a mechanical analysis using classical theories [7], or classical theories with material properties extracted from atomistic simulation [4], or by using a multiscale approach [25].

Algorithm 2. Procedure for coupled electromechanical analysis by using a Lagrangian approach for both mechanical and electrostatic analysis

repeat
1. Do mechanical analysis (on the undeformed geometry) to compute structural displacements
2. Compute charge distribution in the semiconductor by electrostatic analysis (on the undeformed geometry)
3. Compute electrostatic forces (on the undeformed geometry)
until an equilibrium state is reached

The rest of the paper is organized as follows: Section 2 presents a brief description of the hybrid BIE/Poisson/Schrödinger approach for electrostatic analysis of nanostructures, Section 3 presents the Lagrangian hybrid BIE/Poisson/Schrödinger formulations, Section 4 describes the numerical implementation of the Lagrangian hybrid BIE/Poisson approach, Section 5 presents numerical results and Section 6 presents conclusions.

2. Hybrid BIE/Poisson/Schrödinger approach

To explain electrostatic analysis of NEMS, we consider a nanoswitch example as shown in Fig. 1. The nanoswitch consists of a semiconductor beam structure that is clamped

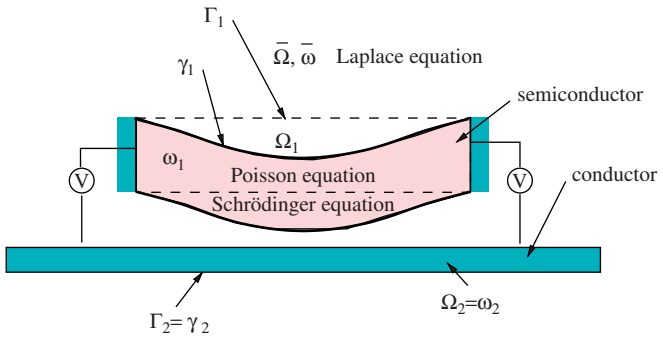

Fig. 1. A typical nanoswitch example consisting of a deformable fixed–fixed semiconductor beam and a fixed bottom conductor.

at the ends and the beam is separated from a bottom conductor/electrode by a small gap. When a voltage is applied between the fixed–fixed beam and the bottom conductor, electrostatic charges are induced in the semiconductor beam. These charges give rise to an electrostatic force, which acts on the entire (surface as well as in the interior) semiconductor beam. Since the bottom conductor is fixed and cannot move, the electrostatic forces deform only the fixed–fixed beam.

The nanoswitch example shown in Fig. 1 contains three regions: the semiconductor structure, the bottom conductor and the infinite dielectric medium that is exterior to the semiconductor structure and the bottom conductor. As shown in Fig. 1, the original undeformed geometry of the semiconductor is denoted as Ω_1 (shown as the dashed line in Fig. 1) and its boundary is Γ_1. The deformed geometry of the semiconductor is denoted as ω_1 and the boundary of the deformed semiconductor is denoted as γ_1. The fixed bottom conductor and its boundary are denoted by Ω_2 (or ω_2) and Γ_2 (or γ_2), respectively. Note that since the bottom conductor cannot move, $\Omega_2 = \omega_2$ and $\Gamma_2 = \gamma_2$. The infinite dielectric medium exterior to the undeformed semiconductor and the bottom conductor is denoted by $\bar{\Omega}$ and the region exterior to the deformed semiconductor and the bottom conductor is denoted by $\bar{\omega}$. The bottom conductor is treated as an equipotential region.

Let us first consider electrostatic analysis of the nanoswitch using the deformed position of the beam. Based on the idealization that the dielectric medium is a perfect insulator, i.e., there is no charge in the entire dielectric medium, the electric potential satisfies the Laplace equation in the dielectric medium (the region exterior to the semiconductor beam and the fixed bottom conductor). The Laplace equation is given by

$$\nabla^2 \phi = 0 \quad \text{in } \bar{\omega}, \tag{1}$$

$$\phi = g(\mathbf{x}) \quad \text{on } \gamma_g, \tag{2}$$

$$q = \frac{\partial \phi}{\partial \mathbf{n}} = h(\mathbf{x}) \quad \text{on } \gamma_h, \tag{3}$$

where $\mathbf{x}^{\mathrm{T}} = \{x, y\}$ is the position vector of a point, and $g(\mathbf{x})$ and $h(\mathbf{x})$ are the potential and its normal derivative specified on the boundary portions γ_g and γ_h ($\gamma_g \cup \gamma_h = \gamma_1 \cup \Gamma_2$) of the semiconductor/conductor structures, respectively. When the critical length (e.g., the width) of the semiconductor structure is comparable to the Debye length or the screening length [26], the potential inside the semiconductor beam satisfies the Poisson equation, which is given by [26]

$$\nabla \cdot (\varepsilon_s \nabla \phi) = \rho = -e(p - n + N_D^+ - N_A^-) \quad \text{in } \omega_1, \tag{4}$$

where e is the elementary charge, ρ is the net charge density, ε_s is the permittivity of the semiconductor material, N_D^+ and N_A^- are the concentration of the ionized donor and acceptor dopants, respectively, and p and n are the hole and electron concentrations, respectively. As the size of the semiconductor structure continues to shrink to nano and sub-nanometer scales, quantum effects become more significant and can even dominate the entire device behavior [10]. The carrier quantum confinement in the semiconductor structure can impose a significant effect on the charge distribution in the mechanical components of NEMS. In this case, the Poisson equation given in Eq. (4) needs to be solved self-consistently with the Schrödinger equation in the semiconductor structure to obtain the potential field and the charge distribution. The two dimensional effective mass Schrödinger equation is given by [27]

$$\begin{aligned} \hat{H}(\psi_n) &= -\left(\frac{\hbar^2}{2m_x^*}\frac{\partial^2}{\partial x^2} + \frac{\hbar^2}{2m_y^*}\frac{\partial^2}{\partial y^2}\right)\psi_n + U(e\phi)\psi_n \\ &= E_n \psi_n \quad \text{in } \omega_1, \end{aligned} \tag{5}$$

where $\hat{H}$ is the Hamiltonian, $\hbar$ is the Planck's constant, m_x^* and m_y^* are the effective masses of an electron or hole in the x- and y-direction, respectively, U is the potential energy and ψ_n is the wave function corresponding to the energy level E_n. In this paper, we employ $U(e\phi) = E_g/2 - e\phi$ for electrons and $U(e\phi) = -E_g/2 - e\phi$ for holes, where E_g is the energy gap. By solving the Schrödinger equation (Eq. (5)), the energy levels E_n and the corresponding wave functions ψ_n can be obtained for electrons and holes. The Poisson equation is coupled with the Schrödinger equation through the quantum electron and hole densities,

$$p(\phi) = N_p \sum_n \psi_n^2 \mathscr{F}_{-1/2}\left(\frac{E_n - E_F}{k_B T}\right), \tag{6}$$

$$n(\phi) = N_n \sum_n \psi_n^2 \mathscr{F}_{-1/2}\left(\frac{E_F - E_n}{k_B T}\right), \tag{7}$$

where E_F is the Fermi level energy, k_B is the Boltzmann constant, T is the temperature, $\mathscr{F}_{-1/2}$ is the complete Fermi–Dirac integral of order $-\frac{1}{2}$ and

$$N_n = \frac{1}{\pi}\left(\frac{2m_{nv}^* k_B T}{\hbar^2}\right)^{1/2}, \quad N_p = \frac{1}{\pi}\left(\frac{2m_{pv}^* k_B T}{\hbar^2}\right)^{1/2}, \tag{8}$$

where m^*_{nv} and m^*_{pv} are the density-of-state masses of electrons and holes, respectively. For two-dimensional quantum confinement, m^*_{nv} and m^*_{pv} are equal to the electron and hole effective masses in the z-direction (denoted by m^*_z), respectively. Fig. 1 shows the regions where the Laplace and the Poisson/Schrödinger equations are solved.

In [13], we have proposed a hybrid technique to solve the governing equations (Eqs. (1), (4), (5)). The key idea in the hybrid technique is to solve the Laplace equation in the exterior domain by using a boundary integral formulation, and then to combine the boundary integral equations (BIEs) with the Poisson/Schrödinger equations for the interior domain analysis of the semiconductor structure(s). In the hybrid approach, the BIEs are satisfied at the boundary nodes of the beam and the fixed conductor (see Fig. 2) and the Poisson/Schrödinger equations are satisfied at the interior nodes of the semiconductor beam. The BIEs are given by

$$\alpha(\mathbf{x})\phi(\mathbf{x}) = \sum_{j=1}^{N_0} \int_{\gamma_j} \phi(\mathbf{x}') \frac{\partial G(\mathbf{x},\mathbf{x}')}{\partial \mathbf{n}'} \,\mathrm{d}\gamma(\mathbf{x}') - \sum_{j=1}^{N_0} \int_{\gamma_j} q(\mathbf{x}') G(\mathbf{x},\mathbf{x}') \,\mathrm{d}\gamma(\mathbf{x}') + \phi_\infty, \tag{9}$$

$$\sum_{j=1}^{N_0} \int_{\gamma_j} q(\mathbf{x}') \,\mathrm{d}\gamma(\mathbf{x}') = 0, \tag{10}$$

where N_0 is the number of NEM structures (for the example shown in Fig. 2, $N_0 = 2$ (the beam and the fixed conductor)), $\mathbf{x}$ is the source point, $\mathbf{x}'$ is the field point, $G(\mathbf{x},\mathbf{x}')$ is the Green's function, $\mathbf{n}'$ is the outward normal at $\mathbf{x}'$, $q(\mathbf{x}') = \partial\phi(\mathbf{x}')/\partial\mathbf{n}'$ is the flux at the field point $\mathbf{x}'$, $\alpha(\mathbf{x})$ is the corner tensor ($\alpha(\mathbf{x}) = \frac{1}{2}$ for smooth boundaries, see [28] for more details), γ_j is the boundary of the jth structure, and ϕ_∞ is the constant reference potential. In two-dimensions, $G(\mathbf{x},\mathbf{x}') = \ln|\mathbf{x}-\mathbf{x}'|/(2\pi)$, where $|\mathbf{x}-\mathbf{x}'|$ is the distance between the source point $\mathbf{x}$ and the field point $\mathbf{x}'$. Note that the quantities in Eqs. (9), (10) are defined only on the boundary of the semiconductors or conductors. The need to discretize the region exterior to the NEM structures and the requirement of a cut-off box are eliminated by using the BIEs for the exterior domain. The BIEs (Eqs. (9), (10)) are coupled with the Poisson equation through the interface conditions [29]

$$\phi(\mathbf{x})|_{BIE} = \phi(\mathbf{x})|_{Poisson} \quad \text{on } \gamma_{int}, \tag{11}$$

$$\varepsilon_s \left.\frac{\partial\phi(\mathbf{x})}{\partial\mathbf{n}}\right|_{Poisson} + \varepsilon_d q(\mathbf{x})|_{BIE} = \sigma_{int} \quad \text{on } \gamma_{int}, \tag{12}$$

where γ_{int} is the boundary interface between the semiconductor structure and the dielectric medium, $\phi|_{BIE}$ and $\phi|_{Poisson}$ are the potentials computed from the BIE and the Poisson equation, respectively, $q|_{BIE}$ is the normal derivative of the potential from the BIE, ε_d is the permittivity of the dielectric medium and σ_{int} is the charge density on the exposed surface of the semiconductor. In addition, external potentials are applied on the bottom conductor and at the two ends of the semiconductor beam, i.e.,

$$\phi = g_1 \quad \text{on } \gamma_{g1} \text{ and } \gamma_{g2}, \tag{13}$$

$$\phi = g_2 \quad \text{on } \Gamma_2. \tag{14}$$

Therefore, for a given set of boundary conditions, Eqs. (13), (14), the potential field and the charge distribution in the semiconductor can be obtained by solving the BIEs, Eqs. (9), (10), the Poisson equation, Eq. (4), and the Schrödinger equation, Eq. (5), self-consistently. The BIEs (Eqs. (9), (10)) are coupled with the Poisson equation through the interface conditions given in Eqs. (11), (12) and the Poisson equation is coupled with the Schrödinger equation through the quantum hole and electron densities given in Eqs. (6), (7).

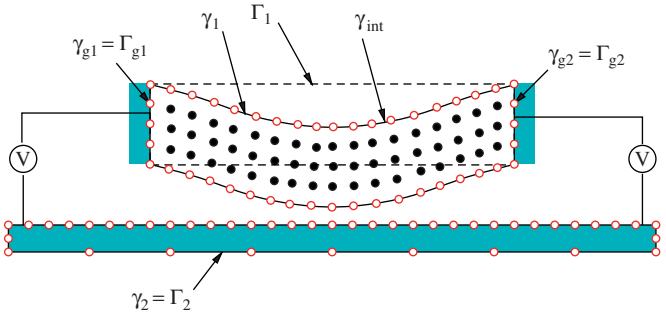

Fig. 2. Hybrid BIE/Poisson/Schrödinger discretization of the nanoswitch example. Γ_1 and γ_1 denote the boundary of the undeformed and the deformed geometry of the semiconductor structure, respectively. γ_{int} is the boundary interface between the semiconductor structure and the dielectric medium. The Poisson/Schrödinger equations are satisfied at the interior nodes (filled circles) of the semiconductor beam and the boundary integral equations and/or the interface conditions are satisfied at the boundary nodes (open circles) of the beam and the fixed conductor.

3. Lagrangian approach

In this section, we introduce a Lagrangian formulation, where the governing BIE, Poisson/Schrödinger equations and the interface conditions defined on the deformed geometries are transformed to the initial or the undeformed configuration of the semiconductors. The governing equations with the Lagrangian description are then solved numerically in the undeformed configuration to compute the electrical potential and the charge density of the deformed semiconductor structure(s).

3.1. Lagrangian description in 2-D: basic concepts

When a material body is subjected to a force, either internal or external, its geometrical shape undergoes a change. As shown in Fig. 3, the initial or the undeformed configuration of a body is denoted by B (all quantities in the initial configuration are denoted by capital letters) and the deformed configuration of the body is denoted by b

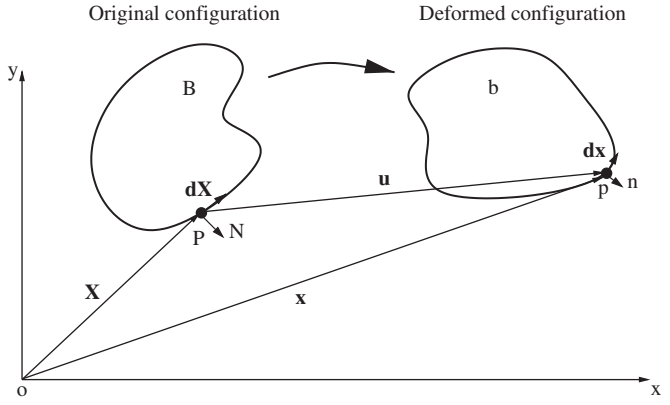

Fig. 3. Various configurations of a deformable body.

(all quantities in the deformed configuration are denoted by lower case letters). Consider an infinitesimal segment on the boundary of B. Let P be the point where the infinitesimal boundary segment is directed from, $\mathbf{X}$ be the position vector of P, $\mathrm{d}\mathbf{X}$ be the vector representing the infinitesimal boundary segment and $\mathbf{N}$ be the unit outward normal at P. When the body deforms from B to b, point P moves to p and its position changes to $\mathbf{x}$. The boundary segment $\mathrm{d}\mathbf{X}$ and the unit outward normal $\mathbf{N}$ in the initial configuration deform to $\mathrm{d}\mathbf{x}$ and $\mathbf{n}$ in the deformed configuration, respectively. Note that the boundary segment changes not only in length but also in direction when it deforms. The displacement from P to p is denoted by vector $\mathbf{u}$. The physical quantities in the deformed configuration can be expressed by the corresponding physical quantities in the initial configuration (Lagrangian description) as described below [30]:

$$\mathbf{x} = \mathbf{X} + \mathbf{u}, \tag{15}$$

$$\mathrm{d}\mathbf{x} = \mathbf{F}\,\mathrm{d}\mathbf{X}, \tag{16}$$

$$\mathrm{d}\mathbf{X} = \mathbf{F}^{-1}\,\mathrm{d}\mathbf{x}, \tag{17}$$

where $\mathbf{F}$ is the deformation gradient tensor given by

$$F_{ij} = \frac{\partial x_i}{\partial X_j} = \delta_{ij} + \frac{\partial u_i}{\partial X_j}, \quad i,j = 1,2 \text{ for 2-}D \tag{18}$$

and the inverse of $\mathbf{F}$ is given by

$$F^{-1}_{ij} = \frac{\partial X_i}{\partial x_j}, \quad i,j = 1,2 \text{ for 2-}D. \tag{19}$$

The components of the position and the displacement vectors are given by

$$\mathbf{x} = \begin{Bmatrix} x \\ y \end{Bmatrix}, \quad \mathbf{X} = \begin{Bmatrix} X \\ Y \end{Bmatrix}, \quad \mathbf{u} = \begin{Bmatrix} u \\ v \end{Bmatrix} \quad \text{for 2-}D. \tag{20}$$

In the initial configuration, the infinitesimal boundary segment $\mathrm{d}\mathbf{X}$ can be represented by the product of its length $\mathrm{d}\Gamma$ and its unit direction vector $\mathbf{T}$. Similarly, the boundary segment, $\mathrm{d}\mathbf{x}$, in the deformed configuration can be represented by the product of its length $\mathrm{d}\gamma$ and its unit direction vector $\mathbf{t}$.

$$\mathrm{d}\mathbf{x} = \mathrm{d}\gamma\mathbf{t}, \tag{21}$$

$$\mathrm{d}\mathbf{X} = \mathrm{d}\Gamma\mathbf{T}. \tag{22}$$

The relation between the unit outward normal at the point $\mathbf{x}$ in the deformed configuration, $\mathbf{n}$, and the unit outward normal at the point $\mathbf{X}$ in the initial configuration, $\mathbf{N}$, is given by Nanson's law [30]

$$\mathbf{n}\,\mathrm{d}\gamma = J\mathbf{F}^{-\mathrm{T}}\mathbf{N}\,\mathrm{d}\Gamma. \tag{23}$$

From Nanson's law and Eqs. (21), (22), we obtain [6,30]

$$\mathrm{d}\gamma = J|\mathbf{F}^{-\mathrm{T}}\mathbf{N}|\,\mathrm{d}\Gamma = (\mathbf{T}\cdot\mathbf{C}\mathbf{T})^{1/2}\,\mathrm{d}\Gamma, \tag{24}$$

where $\mathbf{C} = \mathbf{F}^{\mathrm{T}}\mathbf{F}$ is the Green deformation tensor, $J = \det(\mathbf{F})$, and $\mathbf{T}$ and $\mathbf{N}$ are the unit tangential and the normal vectors, respectively. By using the chain rule and Eq. (19), the gradient of a physical quantity ϕ in the deformed configuration can be expressed as

$$\begin{aligned}\nabla_{\mathbf{x}}\phi &= \begin{Bmatrix} \dfrac{\partial\phi}{\partial x} \\ \dfrac{\partial\phi}{\partial y} \end{Bmatrix} = \begin{Bmatrix} \dfrac{\partial\phi}{\partial X}\dfrac{\partial X}{\partial x} + \dfrac{\partial\phi}{\partial Y}\dfrac{\partial Y}{\partial x} \\ \dfrac{\partial\phi}{\partial X}\dfrac{\partial X}{\partial y} + \dfrac{\partial\phi}{\partial Y}\dfrac{\partial Y}{\partial y} \end{Bmatrix} \\ &= \begin{bmatrix} \dfrac{\partial X}{\partial x} & \dfrac{\partial Y}{\partial x} \\ \dfrac{\partial X}{\partial y} & \dfrac{\partial Y}{\partial y} \end{bmatrix} \begin{Bmatrix} \dfrac{\partial\phi}{\partial X} \\ \dfrac{\partial\phi}{\partial Y} \end{Bmatrix} = \mathbf{F}^{-\mathrm{T}}\nabla_{\mathbf{X}}\phi, \end{aligned} \tag{25}$$

where $\nabla_{\mathbf{X}}\phi$ and $\nabla_{\mathbf{x}}\phi$ denote the gradient of ϕ in the initial and the deformed configurations, respectively. Eq. (25) shows that the differential operator $\nabla_{\mathbf{x}}$ in the deformed configuration can be rewritten in the initial configuration as

$$\nabla_{\mathbf{x}} = \mathbf{F}^{-\mathrm{T}}\nabla_{\mathbf{X}}. \tag{26}$$

The normal derivative of a physical quantity ϕ in the deformed configuration can be rewritten as

$$\begin{aligned}\frac{\partial\phi}{\partial\mathbf{n}} &= \nabla_{\mathbf{x}}\phi\cdot\mathbf{n} = \mathbf{F}^{-\mathrm{T}}\nabla_{\mathbf{X}}\phi\cdot\frac{\mathrm{d}\Gamma}{\mathrm{d}\gamma}\,J\mathbf{F}^{-\mathrm{T}}\mathbf{N} = \mathbf{F}^{-\mathrm{T}}\nabla_{\mathbf{X}}\phi \\ &\quad\cdot\frac{1}{J|\mathbf{F}^{-\mathrm{T}}\mathbf{N}|}\,J\mathbf{F}^{-\mathrm{T}}\mathbf{N} = \mathbf{F}^{-\mathrm{T}}\nabla_{\mathbf{X}}\phi\cdot\frac{\mathbf{F}^{-\mathrm{T}}\mathbf{N}}{|\mathbf{F}^{-\mathrm{T}}\mathbf{N}|} \\ &= \nabla_{\mathbf{X}}\phi\cdot\frac{\mathbf{F}^{-1}\mathbf{F}^{-\mathrm{T}}\mathbf{N}}{|\mathbf{F}^{-\mathrm{T}}\mathbf{N}|} = \nabla_{\mathbf{X}}\phi\cdot\frac{\mathbf{C}^{-1}\mathbf{N}}{|\mathbf{F}^{-\mathrm{T}}\mathbf{N}|} = \frac{\mathbf{C}^{-\mathrm{T}}}{|\mathbf{F}^{-\mathrm{T}}\mathbf{N}|}\frac{\partial\phi}{\partial\mathbf{N}}. \end{aligned} \tag{27}$$

By using the above relations, the geometry of a deformed structure and the differential operators defined on the deformed structure can be expressed in terms of the geometry and the differential operators in the initial configuration and its deformation information.

3.2. Lagrangian form of the hybrid BIE/Poisson/Schrödinger equations

In the Lagrangian approach, we first transform the BIEs, Eqs. (9), (10), to the initial configuration by representing

each component in Eqs. (9), (10) by its counterpart in the initial configuration. Using Eq. (15), the Green's function in two dimensions, $G(\mathbf{x},\mathbf{x}')$, can be rewritten as

$$G(\mathbf{x},\mathbf{x}') = G(\mathbf{x}(\mathbf{X}),\mathbf{x}'(\mathbf{X}')) = \frac{1}{2\pi}\ln|\mathbf{X}-\mathbf{X}'+\mathbf{u}-\mathbf{u}'|, \tag{28}$$

where $\mathbf{X}$ and $\mathbf{X}'$ are the source and the field points in the initial configuration corresponding to the source and the field points $\mathbf{x}$ and $\mathbf{x}'$ in the deformed configuration, $\mathbf{x}(\mathbf{X})$ denotes $\mathbf{x}$ in the deformed configuration mapped to $\mathbf{X}$ in the initial configuration with the mapping $\mathbf{x}=\mathbf{X}+\mathbf{u}$, and $\mathbf{u}$ and $\mathbf{u}'$ are the displacements of points $\mathbf{X}$ and $\mathbf{X}'$, respectively. For coupled electromechanical analysis, these displacements are computed by a mechanical analysis. The normal derivative of the Green's function can be rewritten as

$$\begin{aligned}\frac{\partial G(\mathbf{x},\mathbf{x}')}{\partial \mathbf{n}'} &= \nabla_{\mathbf{x}'}G(\mathbf{x},\mathbf{x}')\cdot\mathbf{n}' \\ &= \frac{1}{2\pi}\begin{Bmatrix} -\dfrac{x-x'}{|\mathbf{x}-\mathbf{x}'|^2} \\ -\dfrac{y-y'}{|\mathbf{x}-\mathbf{x}'|^2}\end{Bmatrix}\cdot\mathbf{n}' = \frac{1}{2\pi}\begin{Bmatrix} -\dfrac{X-X'+u-u'}{|\mathbf{X}-\mathbf{X}'+\mathbf{u}-\mathbf{u}'|^2} \\ -\dfrac{Y-Y'+v-v'}{|\mathbf{X}-\mathbf{X}'+\mathbf{u}-\mathbf{u}'|^2}\end{Bmatrix}\cdot\mathbf{n}' \\ &= \nabla_{\mathbf{X}'}G(\mathbf{x}(\mathbf{X}),\mathbf{x}'(\mathbf{X}'))\cdot\mathbf{n}'.\end{aligned} \tag{29}$$

By using Eq. (24), the Lagrangian form of the second term on the right-hand side of the BIE, Eq. (9), is given by [6]

$$\begin{aligned}&\sum_{j=1}^{N_0}\int_{\gamma_j} q(\mathbf{x}')G(\mathbf{x},\mathbf{x}')\,\mathrm{d}\gamma(\mathbf{x}') \\ &\quad=\sum_{j=1}^{N_0}\int_{\Gamma_j} G(\mathbf{x}(\mathbf{X}),\mathbf{x}'(\mathbf{X}'))q(\mathbf{x}'(\mathbf{X}')) \\ &\qquad\times[\mathbf{T}(\mathbf{X}')\cdot\mathbf{C}(\mathbf{X}')\mathbf{T}(\mathbf{X}')]^{1/2}\,\mathrm{d}\Gamma(\mathbf{X}'),\end{aligned} \tag{30}$$

where $q(\mathbf{x}'(\mathbf{X}'))$ is the flux at a point $\mathbf{x}'$ in the deformed configuration mapped to the point $\mathbf{X}'$ in the initial configuration. By using Eqs. (23), (29), the Lagrangian form of the first term on the right-hand side of the BIE, Eq. (9), can be rewritten as

$$\begin{aligned}&\sum_{j=1}^{N_0}\int_{\gamma_j}\phi(\mathbf{x}')\frac{\partial G(\mathbf{x},\mathbf{x}')}{\partial\mathbf{n}'}\,\mathrm{d}\gamma(\mathbf{x}') \\ &\quad=\sum_{j=1}^{N_0}\int_{\gamma_j}\phi(\mathbf{x}'(\mathbf{X}'))\nabla_{\mathbf{X}'}G(\mathbf{x}(\mathbf{X}),\mathbf{x}'(\mathbf{X}'))\cdot\mathbf{n}'\,\mathrm{d}\gamma(\mathbf{x}') \\ &\quad=\sum_{j=1}^{N_0}\int_{\Gamma_j}\phi(\mathbf{x}'(\mathbf{X}'))\nabla_{\mathbf{X}'}G(\mathbf{x}(\mathbf{X}),\mathbf{x}'(\mathbf{X}'))\cdot J\underline{(}\mathbf{X}')\mathbf{F}^{-\mathrm{T}}(\mathbf{X}') \\ &\qquad\times\mathbf{N}(\mathbf{X}')\,\mathrm{d}\Gamma(\mathbf{X}').\end{aligned} \tag{31}$$

Substituting Eqs. (30), (31) into Eq. (9), the Lagrangian form of the first BIE is given by

$$\begin{aligned}&\alpha(\mathbf{x}(\mathbf{X}'))\phi(\mathbf{x}(\mathbf{X}')) \\ &\quad=\sum_{j=1}^{N_0}\int_{\Gamma_j}\phi(\mathbf{x}'(\mathbf{X}'))\nabla_{\mathbf{X}'}G(\mathbf{x}(\mathbf{X}),\mathbf{x}'(\mathbf{X}'))\cdot J(\mathbf{X}')\mathbf{F}^{-\mathrm{T}}(\mathbf{X}') \\ &\qquad\times\mathbf{N}(\mathbf{X}')\,\mathrm{d}\Gamma(\mathbf{X}') - \sum_{j=1}^{N_0}\int_{\Gamma_j}G(\mathbf{x}(\mathbf{X}),\mathbf{x}'(\mathbf{X}'))q(\mathbf{x}'(\mathbf{X}')) \\ &\qquad\times[\mathbf{T}(\mathbf{X}')\cdot\mathbf{C}(\mathbf{X}')\mathbf{T}(\mathbf{X}')]^{1/2}\,\mathrm{d}\Gamma(\mathbf{X}') + \phi_\infty,\end{aligned} \tag{32}$$

where $\phi(\mathbf{x}'(\mathbf{X}'))$ is the potential at a point $\mathbf{x}'$ in the deformed configuration mapped to the corresponding point $\mathbf{X}'$ in the initial configuration and $\alpha(\mathbf{x}(\mathbf{X}'))$ is the corner tensor in the initial configuration. Note that in the initial configuration ϕ_∞ remains as the same constant and $\alpha(\mathbf{x}(\mathbf{X}'))$ is computed by using the summation rule [28]. The Lagrangian form of Eq. (10) is given by

$$\sum_{j=1}^{N_0}\int_{\Gamma_j} q(\mathbf{x}'(\mathbf{X}'))[\mathbf{T}(\mathbf{X}')\cdot\mathbf{C}(\mathbf{X}')\mathbf{T}(\mathbf{X}')]^{1/2}\,\mathrm{d}\Gamma(\mathbf{X}') = 0. \tag{33}$$

Next, we transform the Poisson equation (Eq. (4)) from the deformed configuration to the initial configuration. Substituting Eq. (26) into Eq. (4), the Poisson equation can be rewritten in the Lagrangian form as

$$\begin{aligned}&(\mathbf{F}^{-\mathrm{T}}(\mathbf{X})\nabla_{\mathbf{X}})\cdot(\varepsilon_s(\mathbf{x}(\mathbf{X}))\mathbf{F}^{-\mathrm{T}}(\mathbf{X})\nabla_{\mathbf{X}}\phi(\mathbf{x}(\mathbf{X}))) \\ &\quad=-e(p(\mathbf{x}(\mathbf{X}))-n(\mathbf{x}(\mathbf{X}))+N_D^+-N_A^-).\end{aligned} \tag{34}$$

Assuming ε_s is a constant, Eq. (34) can be rewritten as

$$\begin{aligned}&\varepsilon_s[(\mathbf{F}^{-\mathrm{T}}(\mathbf{X})\nabla_{\mathbf{X}})\cdot(\mathbf{F}^{-\mathrm{T}}(\mathbf{X})\nabla_{\mathbf{X}}\phi(\mathbf{x}(\mathbf{X})))] \\ &\quad=-e(p(\mathbf{x}(\mathbf{X}))-n(\mathbf{x}(\mathbf{X}))+N_D^+-N_A^-).\end{aligned} \tag{35}$$

It can be easily shown that Eq. (35) can also be rewritten as

$$\begin{aligned}&\frac{\varepsilon_s}{J(\mathbf{X})}[\nabla_{\mathbf{X}}\cdot(J(\mathbf{X})\mathbf{C}^{-1}(\mathbf{X})\nabla_{\mathbf{X}}\phi(\mathbf{x}(\mathbf{X})))] \\ &\quad=-e(p(\mathbf{x}(\mathbf{X}))-n(\mathbf{x}(\mathbf{X}))+N_D^+-N_A^-).\end{aligned} \tag{36}$$

Note that in Eq. (36) all the quantities are mapped to the initial or the undeformed configuration. Similarly, the Lagrangian form of the Schrödinger equation (Eq. (5)) is given by

$$\begin{aligned}&-\frac{\hbar^2}{2}[(\mathbf{F}^{-\mathrm{T}}(\mathbf{X})\nabla_{\mathbf{X}})\cdot(\mathbf{F}_m^{-\mathrm{T}}(\mathbf{X})\nabla_{\mathbf{X}}\psi_n(\mathbf{x}(\mathbf{X})))] \\ &\quad+U(e\phi(\mathbf{x}(\mathbf{X})))\psi_n(\mathbf{x}(\mathbf{X}))=E_n(\mathbf{x}(\mathbf{X}))\psi_n(\mathbf{x}(\mathbf{X})),\end{aligned} \tag{37}$$

where $E_n(\mathbf{x}(\mathbf{X}))$ and $\psi_n(\mathbf{x}(\mathbf{X}))$ are the eigen-energy and the wave function of the semiconductor in the deformed configuration mapped to the initial configuration, and

$$\mathbf{F}_m^{-\mathrm{T}}(\mathbf{X}) = \begin{bmatrix} m_x^* F_{11}^{-1}(\mathbf{X}) & m_x^* F_{21}^{-1}(\mathbf{X}) \\ m_y^* F_{12}^{-1}(\mathbf{X}) & m_y^* F_{22}^{-1}(\mathbf{X})\end{bmatrix}. \tag{38}$$

The quantum electron and hole densities are given by

$$n(\phi(\mathbf{x}(\mathbf{X}))) = N_n\sum_n \psi_n^2(\mathbf{x}(\mathbf{X}))\mathscr{F}_{-1/2}\left(\frac{E_F-E_n(\mathbf{x}(\mathbf{X}))}{k_BT}\right), \tag{39}$$

$$p(\phi(\mathbf{x}(\mathbf{X}))) = N_p\sum_n \psi_n^2(\mathbf{x}(\mathbf{X}))\mathscr{F}_{-1/2}\left(\frac{E_n(\mathbf{x}(\mathbf{X}))-E_F}{k_BT}\right). \tag{40}$$

Substituting Eq. (27) into Eq. (12), the Lagrangian form of the interface conditions given in Eqs. (11), (12) is given by

$$\phi(\mathbf{x}(\mathbf{X}))|_{BIE} = \phi(\mathbf{x}(\mathbf{X}))|_{Poisson} \quad \text{on } \Gamma_{int}, \tag{41}$$

$$\varepsilon_s \frac{\nabla_{\mathbf{X}}\phi(\mathbf{x}(\mathbf{X})) \cdot \mathbf{C}^{-1}(\mathbf{X})\mathbf{N}(\mathbf{X})}{|\mathbf{F}^{-\mathrm{T}}(\mathbf{X})\mathbf{N}(\mathbf{X})|}|_{Poisson} + \varepsilon_d q(\mathbf{x}(\mathbf{X}))|_{BIE} = \sigma_{int}(\mathbf{x}(\mathbf{X})) \quad \text{on } \Gamma_{int}. \tag{42}$$

The boundary conditions given in Eqs. (13), (14) remain the same as the applied potential does not change with the structural deformation, i.e.,

$$\phi(\mathbf{X}) = g_1 \quad \text{on } \Gamma_{g1} \text{ and } \Gamma_{g2}, \tag{43}$$

$$\phi(\mathbf{X}) = g_2 \quad \text{on } \Gamma_2. \tag{44}$$

In summary, the Lagrangian form of the hybrid BIE/Poisson/Schrödinger equations are given by Eqs. (32), (33), (35), (37) along with the interface and the boundary conditions given in Eqs. (41)–(44). As shown in Fig. 4, the Lagrangian form of the hybrid equations are solved in the initial or in the undeformed configuration to obtain the potential, charge density, energy levels and the wavefunctions on the deformed position of the semiconductor structure(s). Once the potential and the charge density are computed, the electrostatic body force in the initial configuration of the semiconductor structure can be computed by [31]

$$\mathbf{B}_{elec} = J\rho\nabla_{\mathbf{x}}\phi = J\rho\mathbf{F}^{-\mathrm{T}}\nabla_{\mathbf{X}}\phi, \tag{45}$$

where $\mathbf{B}_{elec}$ denotes the electrostatic body force and ρ is the charge density as defined in Eq. (4). The electrostatic pressure, $\mathbf{H}$, on the beam surface in the initial configuration is given by [7]

$$\mathbf{H} = \frac{\sigma_{int}^2}{2\varepsilon_d} J\mathbf{F}^{-\mathrm{T}}\mathbf{N}. \tag{46}$$

Remarks.

1. The Lagrangian approach is mathematically equivalent to the deformed configuration approach discussed in Section 2. However, the Lagrangian approach possesses several advantages compared to the deformed configuration approach: (1) it does not require any update of the geometry of the structures; (2) it eliminates integration error that arises when flat panels are used to approximate curved surfaces; and (3) interpolation functions need not be re-computed whenever a structure undergoes a shape change.
2. In this section, the Lagrangian form of the BIE/Poisson/Schrödinger equations are derived for quantum-mechanical electrostatic analysis of NEMS. As the semiclassical electrostatic analysis [13] is a special case of the quantum-mechanical electrostatic analysis, the Lagrangian formulation can be easily extended for the semiclassical electrostatic analysis.
3. The deformation quantities in the Hamiltonian of the Lagrangian Schrödinger equation (Eq. (37)) change as the structure deforms. Since the deformation quantities are the coefficients of the differential operator in the Hamiltonian, the eigen-energies and the wavefunctions for a new deformation can be computed easily using a perturbation technique [27]. This, however, is computationally more expensive in the deformed configuration approach.
4. Deformation of the NEM structure(s) can also arise due to other sources such as thermal effects [32] or fabrication errors [33]. Regardless of the source, if the deformation of the structure(s) is known, the electrostatic analysis can be performed on the undeformed geometry of the structure(s) by using the Lagrangian formulation.
5. In a general coupled electrostatic and mechanical analysis, the mechanical deformation of the structures can be computed by using various numerical methods, where the displacement field is approximated by interpolation or shape functions. The deformation gradient, which contains the derivatives of the displacements, is typically obtained by using the same set of shape functions. When the displacements are approximated by linear shape functions (i.e., $\mathbf{F}$ is constant within each boundary panel), the deformed configuration approach and the Lagrangian approach give identical solutions. This result has been shown in [6]. However, when the displacements are nonlinear, the originally flat boundary typically becomes curved. The nonlinear displacements can be described accurately by using a higher order approximation of the displacements and $\mathbf{F}$, whereas the use of flat panels in the deformed configuration approach is a lower order approximation to the displacements. Therefore, the Lagrangian approach is typically more accurate than the deformed configuration approach.
6. In coupled electromechanical analysis of NEMS, one typically needs to perform electrostatic analysis repeatedly for different deformations of the semiconductor structure. In this case, a sensitivity analysis [34] can be employed with the Lagrangian BIE/Poisson/Schrödinger equations given in Eqs. (32), (33), (35), (37) to speed-up the calculations.

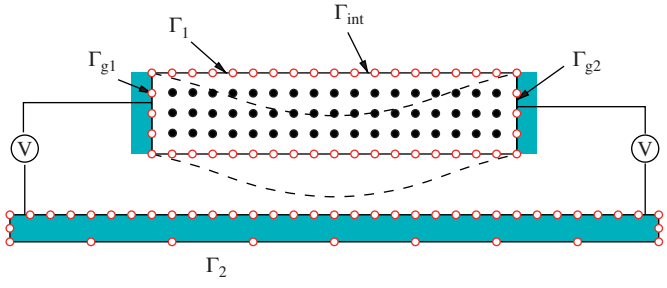

Fig. 4. Lagrangian hybrid BIE/Poisson/Schrödinger discretization of the nanoswitch domain. The discretization of the deformed position (indicated by the dashed line) of the semiconductor structure is not required in this approach.

4. Numerical implementation

In our implementation of the Lagrangian form of the hybrid BIE/Poisson/Schrödinger equations, the undeformed semiconductor structure and the surface of the bottom conductor are discretized into points/nodes, as shown in Fig. 4. We then employ a FCM [17–20] to solve the Lagrangian form of the Poisson and the Schrödinger equations (Eqs. (35), (37)) for the interior nodes of the semiconductor beam and a boundary cloud method (BCM) [21,22] to solve the BIEs given in Eqs. (32), (33) for the boundary nodes of the semiconductor structure and the fixed conductor. The FCM is a meshless method (see e.g., [16] for an overview of meshless methods) in which only points are needed to cover the structural domain and no connectivity information among the points is required. The FCM uses a fixed kernel technique to construct the shape functions and a point collocation technique to discretize the governing partial differential equations. In FCM, the unknown potential $\phi(\mathbf{x}(\mathbf{X}))$ and the wave function $\psi_n(\mathbf{x}(\mathbf{X}))$ are approximated using the shape functions by

$$\begin{aligned}\phi(\mathbf{x}(\mathbf{X})) &\approx \phi^a(\mathbf{x}(\mathbf{X})) = \sum_{I=1}^{NS} N_I(\mathbf{X})\hat{\phi}_I,\\ \psi_n(\mathbf{x}(\mathbf{X})) &\approx \psi_n^a(\mathbf{x}(\mathbf{X})) = \sum_{I=1}^{NS} N_I(\mathbf{X})\hat{\psi}_{nI},\end{aligned} \tag{47}$$

where $\phi^a(\mathbf{x}(\mathbf{X}))$, $\psi_n^a(\mathbf{x}(\mathbf{X}))$ are approximations to $\phi(\mathbf{x}(\mathbf{X}))$ and $\psi_n(\mathbf{x}(\mathbf{X}))$, respectively, and the derivatives of $\phi(\mathbf{x}(\mathbf{X}))$ and $\psi_n(\mathbf{x}(\mathbf{X}))$ are approximated by

$$\begin{aligned}\frac{\partial\phi}{\partial X}(\mathbf{x}(\mathbf{X})) &\approx \frac{\partial\phi^a}{\partial X}(\mathbf{x}(\mathbf{X})) = \sum_{I=1}^{NS}\frac{\partial N_I}{\partial X}(\mathbf{X})\hat{\phi}_I,\\ \frac{\partial^2\phi}{\partial X^2}(\mathbf{x}(\mathbf{X})) &\approx \frac{\partial^2\phi^a}{\partial X^2}(\mathbf{x}(\mathbf{X})) = \sum_{I=1}^{NS}\frac{\partial^2 N_I}{\partial X^2}(\mathbf{X})\hat{\phi}_I,\end{aligned} \tag{48}$$

$$\begin{aligned}\frac{\partial\psi_n}{\partial X}(\mathbf{x}(\mathbf{X})) &\approx \frac{\partial\psi_n^a}{\partial X}(\mathbf{x}(\mathbf{X})) = \sum_{I=1}^{NS}\frac{\partial N_I}{\partial X}(\mathbf{X})\hat{\psi}_{nI},\\ \frac{\partial^2\psi_n}{\partial X^2}(\mathbf{x}(\mathbf{X})) &\approx \frac{\partial^2\psi_n^a}{\partial X^2}(\mathbf{x}(\mathbf{X})) = \sum_{I=1}^{NS}\frac{\partial^2 N_I}{\partial X^2}(\mathbf{X})\hat{\psi}_{nI},\end{aligned} \tag{49}$$

where NS is the total number of nodes used to discretize the semiconductor beam, $\hat{\phi}_I$ and $\hat{\psi}_{nI}$ are the nodal parameters for node I, and $N_I(\mathbf{X})$ is the meshless shape function of node I evaluated at $\mathbf{X}$ (see [17–20] for details). In a BCM, the unknown potential $\phi(\mathbf{x}(\mathbf{X}))$ and its normal derivative $q(\mathbf{x}(\mathbf{X}))$ for a boundary point can be approximated by either a Hermite-type approximation [21] or a varying basis least-squares approximation [22]. The shape functions are constructed for the boundary nodes without using a mesh. In this paper, we employ a varying basis least-squares approach to approximate the unknown quantities in the BIEs. The discrete form of the varying basis approximation for the unknowns is given by

$$\phi(\mathbf{x}(\mathbf{X})) \approx \phi^a(\mathbf{x}(\mathbf{X})) = \sum_{I=1}^{NB}\overline{N}_I(\mathbf{X})\tilde{\phi}_I, \tag{50}$$

$$q(\mathbf{x}(\mathbf{X})) \approx q^a(\mathbf{x}(\mathbf{X})) = \sum_{I=1}^{NB}\overline{N}_I(\mathbf{X})\tilde{q}_I, \tag{51}$$

where NB is the number of boundary points, $\tilde{\phi}_I$ and $\tilde{q}_I$ are the BCM nodal parameters of ϕ and q for node I, respectively, and $\overline{N}_I(\mathbf{X})$ is the shape function of node I (see [22] for details). The boundary of the structure is discretized into NC cells for integration purpose. Each cell contains a certain number of nodes and the number of nodes can vary from cell to cell.

After the shape functions are constructed, both the FCM and the BCM use a point collocation technique to discretize the governing equations. In a point collocation approach, the governing equations are satisfied at every node which does not carry a boundary condition, and for nodes with boundary conditions the approximate solution or the derivative of the approximate solution are set to the given Dirichlet and Neumann boundary conditions, respectively. In FCM, the approximations of the unknown quantities given in Eqs. (47)–(49) are substituted into Eqs. (35), (37), (41)–(44) to satisfy the Lagrangian form of the Poisson equation, the Schrödinger equation and the boundary/interface conditions for the points on the semiconductor. In BCM, the approximations of the unknown quantities given in Eqs. (50), (51) are substituted into Eqs. (32), (33), (41)–(44) to satisfy the Lagrangian BIEs and the boundary/interface conditions for the boundary points. The discretized Lagrangian form of the Poisson equation, Eq. (35), for an interior node $\mathbf{X}_i$ in the initial configuration is given by

$$\begin{aligned}&\varepsilon_s\sum_{I=1}^{NS}[(\mathbf{F}^{-\mathrm{T}}\nabla_{\mathbf{X}})\cdot(\mathbf{F}^{-\mathrm{T}}\nabla_{\mathbf{X}}N_I(\mathbf{X}_i))]\hat{\phi}_I\\ &\quad= -e(p(\mathbf{x}(\mathbf{X}_i)) - n(\mathbf{x}(\mathbf{X}_i)) + N_D^+ - N_A^-).\end{aligned} \tag{52}$$

Note that, in Eq. (52) and in the following equations, $\mathbf{F}^{-\mathrm{T}}(\mathbf{X}_i)$, $J(\mathbf{X}_i)$, $\mathbf{N}(\mathbf{X}_i)$, $\mathbf{T}(\mathbf{X}_i)$ and $\mathbf{C}(\mathbf{X}_i)$ are simply denoted by $\mathbf{F}^{-\mathrm{T}}$, J, $\mathbf{N}$, $\mathbf{T}$ and $\mathbf{C}$, respectively, for brevity. The discretized Lagrangian form of the Schrödinger equation, Eq. (37), for a interior node $\mathbf{X}_i$ is given by

$$\begin{aligned}&-\frac{\hbar^2}{2}\sum_{I=1}^{NS}[(\mathbf{F}^{-\mathrm{T}}\nabla_{\mathbf{X}})\cdot(\mathbf{F}_m^{-\mathrm{T}}\nabla_{\mathbf{X}}N_I(\mathbf{X}_i)) + U(e\phi(\mathbf{x}(\mathbf{X}_i)))]\hat{\psi}_{nI}\\ &\quad= E_n(\mathbf{x}(\mathbf{X}_i))\sum_{I=1}^{NS}N_I(\mathbf{X}_i)\hat{\psi}_{nI}.\end{aligned} \tag{53}$$

The discretized Lagrangian form of the BIE, Eq. (32), for a boundary node $\mathbf{X}_i$ is given by

$$\sum_{J=1}^{NB}\left[\alpha\overline{N}_J(\mathbf{X}_i) - \sum_{k=1}^{N_C}\int_{\Gamma_k}\overline{N}_J(\mathbf{X}')\nabla_{\mathbf{X}'}G(\mathbf{x}(\mathbf{X}_i),\mathbf{x}'(\mathbf{X}'))\right.$$

$$\times J\mathbf{F}^{-\mathrm{T}}\mathbf{N}\,\mathrm{d}\Gamma\Bigg]\tilde{\phi}_J = -\sum_{J=1}^{NB}\Bigg[\sum_{k=1}^{N_C}\int_{\Gamma_k} G(\mathbf{x}(\mathbf{X}_i),\mathbf{x}'(\mathbf{X}'))\overline{N}_J(\mathbf{X}') \times[\mathbf{T}\cdot\mathbf{CT}]^{1/2}\,\mathrm{d}\Gamma\Bigg]\tilde{q}_J + \phi_\infty, \tag{54}$$

where Γ_k is the kth cell on the boundary. The discretized BIE, Eq. (33), is given by

$$\sum_{J=1}^{NB}\Bigg[\sum_{k=1}^{NC}\int_{\Gamma_k}\overline{N}_J(\mathbf{X}')[\mathbf{T}\cdot\mathbf{CT}]^{1/2}\,\mathrm{d}\Gamma\Bigg]\tilde{q}_J = 0. \tag{55}$$

The discretized Dirichlet potential boundary condition, Eq. (43), for an FCM boundary node $\mathbf{X}_i$ is given by

$$\sum_{I=1}^{NS} N_I(\mathbf{X}_i)\hat{\phi}_I = g_1(\mathbf{X}_i), \tag{56}$$

the discretized Dirichlet potential boundary condition, Eqs. (43), (44), for a BCM boundary node $\mathbf{X}_i$ is given by

$$\sum_{J=1}^{NB}\overline{N}_J(\mathbf{X}_i)\tilde{\phi}_J = g_j(\mathbf{X}_i),\quad j=1,2 \tag{57}$$

and the discretized Lagrangian form of the interface conditions, Eq. (41), (42), for a boundary node $\mathbf{X}_i$ are given by

$$\sum_{J=1}^{NB}\overline{N}_J(\mathbf{X}_i)\tilde{\phi}_J = \sum_{I=1}^{NS} N_I(\mathbf{X}_i)\hat{\phi}_I, \tag{58}$$

$$\varepsilon_s\frac{\mathbf{C}^{-1}\mathbf{N}}{|\mathbf{F}^{-\mathrm{T}}\mathbf{N}|}\cdot\nabla_{\mathbf{X}}\sum_{I=1}^{NS}N_I(\mathbf{X}_i)\hat{\phi}_I + \varepsilon_d\sum_{J=1}^{NB}\overline{N}_J(\mathbf{X}_i)\tilde{q}_J = \sigma_{int}(\mathbf{x}(\mathbf{X}_i)). \tag{59}$$

Eqs. (52)–(59) give rise to a linear system (see [13] for details)

$$\mathbf{J}(\mathbf{u})\begin{Bmatrix}\delta\hat{\phi}\\ \delta\tilde{\boldsymbol{\phi}}\\ \delta\tilde{\mathbf{q}}\end{Bmatrix} = -\mathbf{R}(E_n,\boldsymbol{\psi}_n) \tag{60}$$

and an eigen-system

$$\mathbf{H}(\phi,\mathbf{u})\hat{\boldsymbol{\psi}}_n = E_n\hat{\boldsymbol{\psi}}_n, \tag{61}$$

where $\mathbf{J}$ is the Jacobian matrix, $\mathbf{u}$ is the displacement vector, $\delta\hat{\phi}$, $\delta\tilde{\boldsymbol{\phi}}$ and $\delta\tilde{\mathbf{q}}$ are the vectors of unknown increments of the nodal parameters and $\mathbf{R}$ is the residual vector. The nodal parameters $\hat{\phi}$, $\tilde{\boldsymbol{\phi}}$, $\hat{\psi}_n$, and $\tilde{\mathbf{q}}$ can be obtained by iteratively solving the coupled equations (60), (61). Once the nodal parameters are obtained, the potential ϕ and its normal derivative q can be computed by using Eqs. (47), (50), (51). The charge distribution in the semiconductor beam structure can then be computed by evaluating the right-hand side of Eq. (4). From the charge distribution the electrostatic forces can be computed by using Eqs. (45), (46).

Remark.

1. The Lagrangian form of the hybrid BIE/Poisson/Schrödinger approach for quantum-mechanical electrostatic analysis described in Section 3 is independent of the numerical methods used. One can use any domain-based numerical method, such as the finite element or the finite difference method, to solve the Lagrangian form of the Poisson and the Schrödinger equations inside the semiconductor structure, and any boundary-based numerical method, such as the boundary element method, to solve the boundary integral equations on the boundary of the NEM structures. In this paper, we solve the Lagrangian form of the BIE/Poisson/Schrödinger equations by employing the meshless techniques as described above.

5. Numerical examples

In this section we perform electrostatic analysis of several nanoswitch examples by using the Lagrangian form of the hybrid BIE/Poisson/Schrödinger approach. In all calculations, we have used $e = 1.6\times10^{-19}\,\mathrm{C}$, $\sigma_{int}=0$, $\hbar = 1.055\times10^{-34}\,\mathrm{Js}$, $E_g = 1.12\,\mathrm{eV}$, $k_B = 1.38066\times10^{-23}\,\mathrm{J/K}$, $T = 300\,\mathrm{K}$, $\varepsilon_d = \varepsilon_0 = 8.85\times10^{-12}\,\mathrm{C^2/N\,m^2}$ and $\varepsilon_s = 11.7\varepsilon_0$, where ε_0 is the permittivity of the vacuum. The electron effective masses are taken to be $m_x^* = 0.19m_0$, $m_y^* = 0.98m_0$ and $m_z^* = 0.19m_0$, and the hole effective masses are $m_x^* = m_y^* = m_z^* = 0.49m_0$ for heavy holes, $m_x^* = m_y^* = m_z^* = 0.16m_0$ for light holes and $m_x^* = m_y^* = m_z^* = 0.29m_0$ for split-off holes, where $m_0 = 9.11\times10^{-31}\,\mathrm{kg}$ is the free electron rest mass. N-type doping is used for all the examples shown in this paper, which means that only the quantization of the electrons is important and the quantum effect of the holes can be neglected. As a result, the Schrödinger equation is solved only for the electrons and, instead of using Eq. (6), the hole concentration is obtained by

$$p = N_V\mathscr{F}_{1/2}\left(\frac{E_V - E_F}{k_BT}\right), \tag{62}$$

where $E_V = -E_g/2 - e\phi$ is the valence band, $N_V = 1.83\times10^{19}/\mathrm{cm}^3$ is the effective density of states of the valence band and $\mathscr{F}_{1/2}$ is the complete Fermi–Dirac integral of order $\frac{1}{2}$. However, other models for the interface charge density can also be implemented. For all the examples, we also compute the charge distribution in the deformed configuration to compare the results obtained from the Lagrangian and the deformed configuration approaches. In addition, since capacitance is often of interest for electromechanical sensors, the capacitance of the nanoswitch is also

computed. Note that, since the focus of this paper is on the development of a Lagrangian approach, rather than the investigation of quantum physics in NEM structures, the Schrödinger equation with a simple effective mass approximation is used in all the examples. However, the Lagrangian approach can be employed for more advanced physical models within the framework of the coupled Poisson/Schrödinger equations.

As a first example, we consider a nanoswitch containing a 20 nm long and a 5 nm wide silicon beam which can move vertically with the side contact. The initial gap between the beam and the bottom conductor is 5 nm. The beam has an N-type doping density of $10^{15}/\mathrm{cm}^3$. The potential on the left end of the beam is specified as 0 V. The applied potential on the bottom conductor is 5 V. The bottom conductor is 40 nm long and 5 nm wide. The nanoswitch is shown in Fig. 5(a). The dashed line represents the initial configuration of the top semiconductor and the solid shape is the deformed shape of the structure. The objective of this example is to compute the charge distribution in the semiconductor beam when the beam undergoes rigid body motion in the y-direction. Note that the bottom conductor is fixed and does not undergo any deformation. The displacement field of the top semiconductor is given by

$$\begin{cases} u = 0 \\ v = a, \quad a = -4, -3, -2, -1, 0, \end{cases} \tag{63}$$

where u is the x-component of the displacement and v is the y-component of the displacement and we consider five different displacements ($a = -4, -3, -2, -1, 0$) giving rise to five different gaps between the beam and the fixed conductor. The system is solved by using both the Lagrangian and the deformed configuration approaches. The charge distributions in the semiconductor obtained by the Lagrangian and the deformed configuration approaches are identical. The charge density profile is shown in Fig. 5(b) for $a = -4$ nm. Fig. 5(c) shows the capacitance variation of the nanoswitch system as a function of the displacement of the semiconductor.

The second example is a nanoswitch with a 20 nm × 5 nm cantilever silicon beam. The initial gap between the beam and the bottom conductor is 5 nm. The beam has an N-type doping density of $10^{15}/\mathrm{cm}^3$. The potential at the left end of the beam is specified as 0 V. The applied potential on the bottom conductor is 5 V. The fixed bottom conductor is 40 nm long and 5 nm wide. The left end of the top

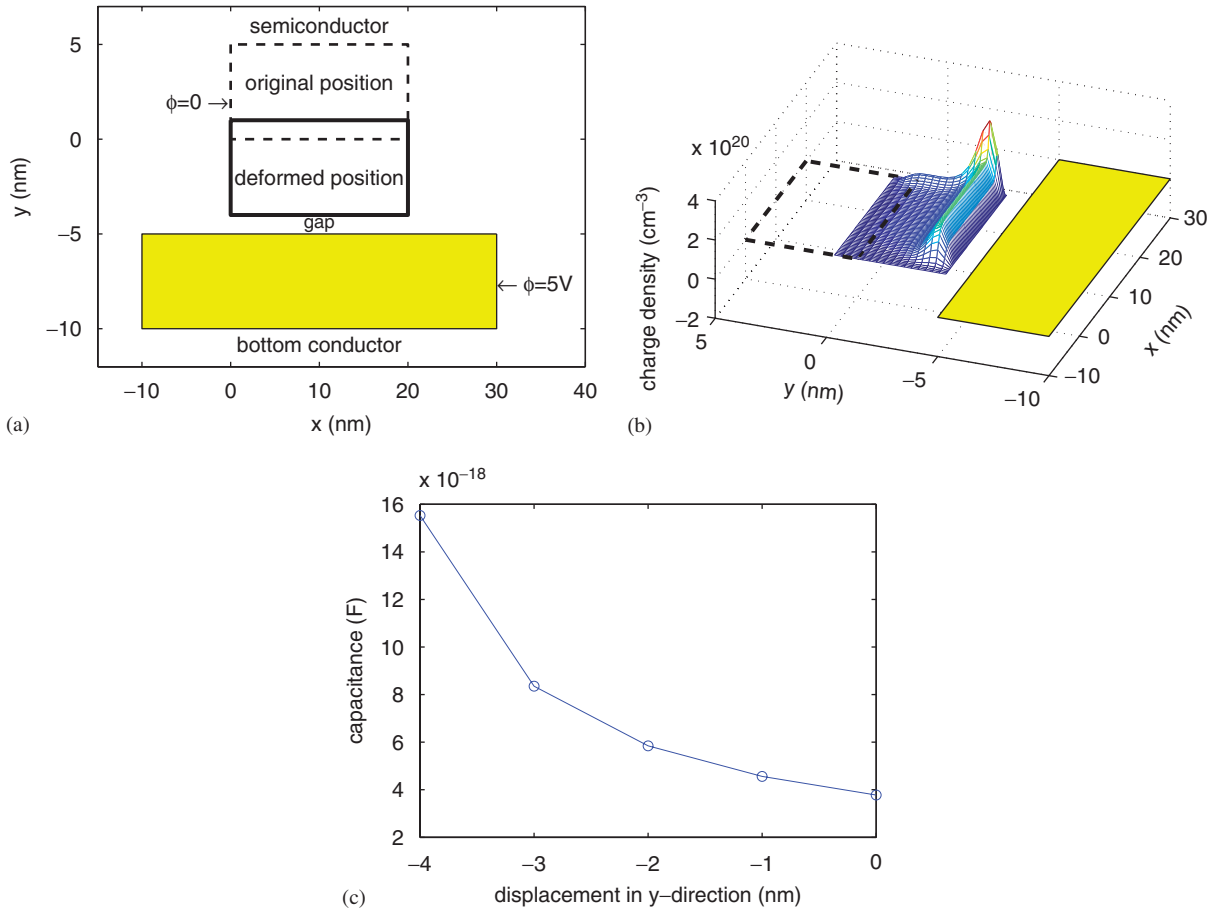

Fig. 5. A simple nanoswitch example: (a) the top semiconductor beam is subjected to a rigid body motion in the y-direction; (b) charge distribution in the deformed semiconductor beam when $a = -4$ nm; (c) capacitance variation as a function of the displacement.

semiconductor is fixed and the beam displacement is given by

$$\begin{cases} u = P(y - D/2)[(6L - 3x)x + 2.25(y^2 - Dy)], \\ v = P\left[0.75\left(y^2 - Dy + \dfrac{D^2}{4}\right)(L - x) + 5.25\dfrac{D^2 x}{4} \right. \\ \qquad \left. +(3L - x)x^2\right], \end{cases} \tag{64}$$

where $L(= 20\,\text{nm})$ and $D(= 5\,\text{nm})$ are the length and the width of the beam, respectively, and by varying $P(-2 \times 10^{-4} \leqslant P \leqslant 0)$ we can change the displacement of the beam. The original and the deformed configurations of the system are shown in Fig. 6(a). The system is solved by using both the Lagrangian and the deformed configuration approaches. The variation of the capacitance with the peak displacement in the y-direction is shown in Fig. 6(b). The charge density computed by the Lagrangian approach and the deformed configuration approach is shown in Fig. 6(c) and (d), respectively. The results look identical (see Fig. 6(b)), but there is a small difference in the solutions obtained by the two approaches as shown in Fig. 6(e). The small error arises because of the geometrical approximations involved in the deformed configuration approach. When a structure deforms or changes shape, the surfaces become curved. When curved surfaces are approximated by

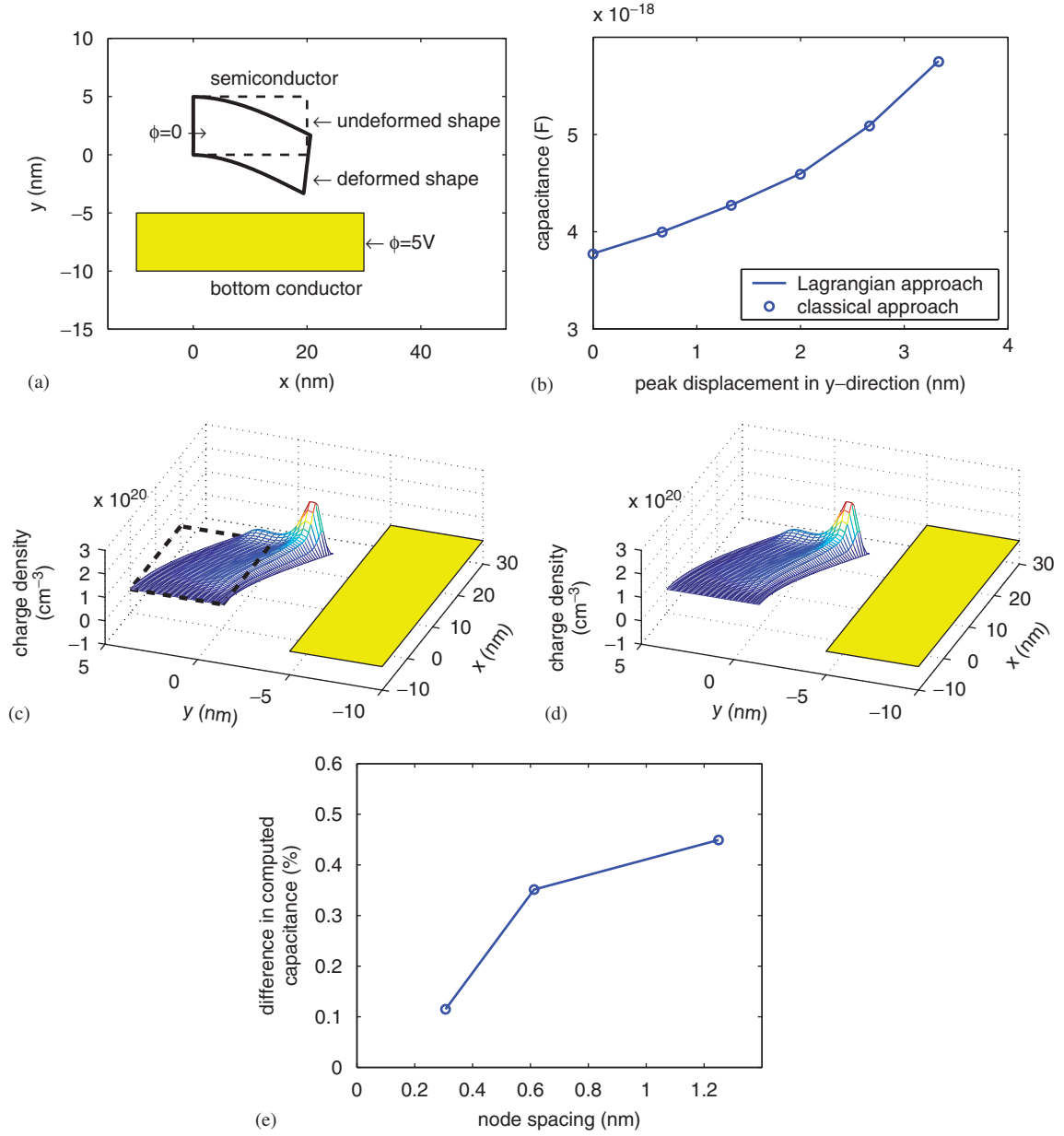

Fig. 6. A cantilever nanoswitch example: (a) the top semiconductor beam is subjected to a bending deformation; (b) capacitance variation as a function of the peak displacement $(-2 \times 10^{-4} \leqslant P \leqslant 0)$; the deformed configuration approach is indicated as the classical approach; (c) charge distribution in the deformed semiconductor beam obtained from the Lagrangian approach; (d) charge distribution in the deformed semiconductor beam obtained from the deformed configuration approach; (e) capacitance difference between the two approaches.

straight cells, numerical errors can be introduced into the deformed configuration approach. Furthermore, the points used to discretize the semiconductor move when the structure deforms. For a uniform point discretization in the initial configuration, the points become non-uniform in the deformed configuration. As a result, the meshless shape functions in the deformed configuration are computed by using the non-uniform distribution of points. A refinement study is performed to investigate the difference in the solution between the two approaches. The top semiconductor is discretized into 16×4, 32×8 and 64×16 points and the boundary of the structures is discretized into 68, 132 and 260 cells, respectively. The capacitance difference between the two approaches is found to be 0.45% for a discretization of 16×4 points and 80 cells. When the semiconductor is discretized into 64×16 points and the boundary of the structures is discretized into 320 cells, the capacitance difference reduced to 0.1%. The error plots are shown in Fig. 6(e). The use of more points/cells reduces the integration error in the deformed configuration approach. Hence the results are closer to the Lagrangian approach. From this example, we can conclude that the Lagrangian approach is more accurate as all the integrations are performed in the initial configuration and the shape functions are computed on a uniform set of points.

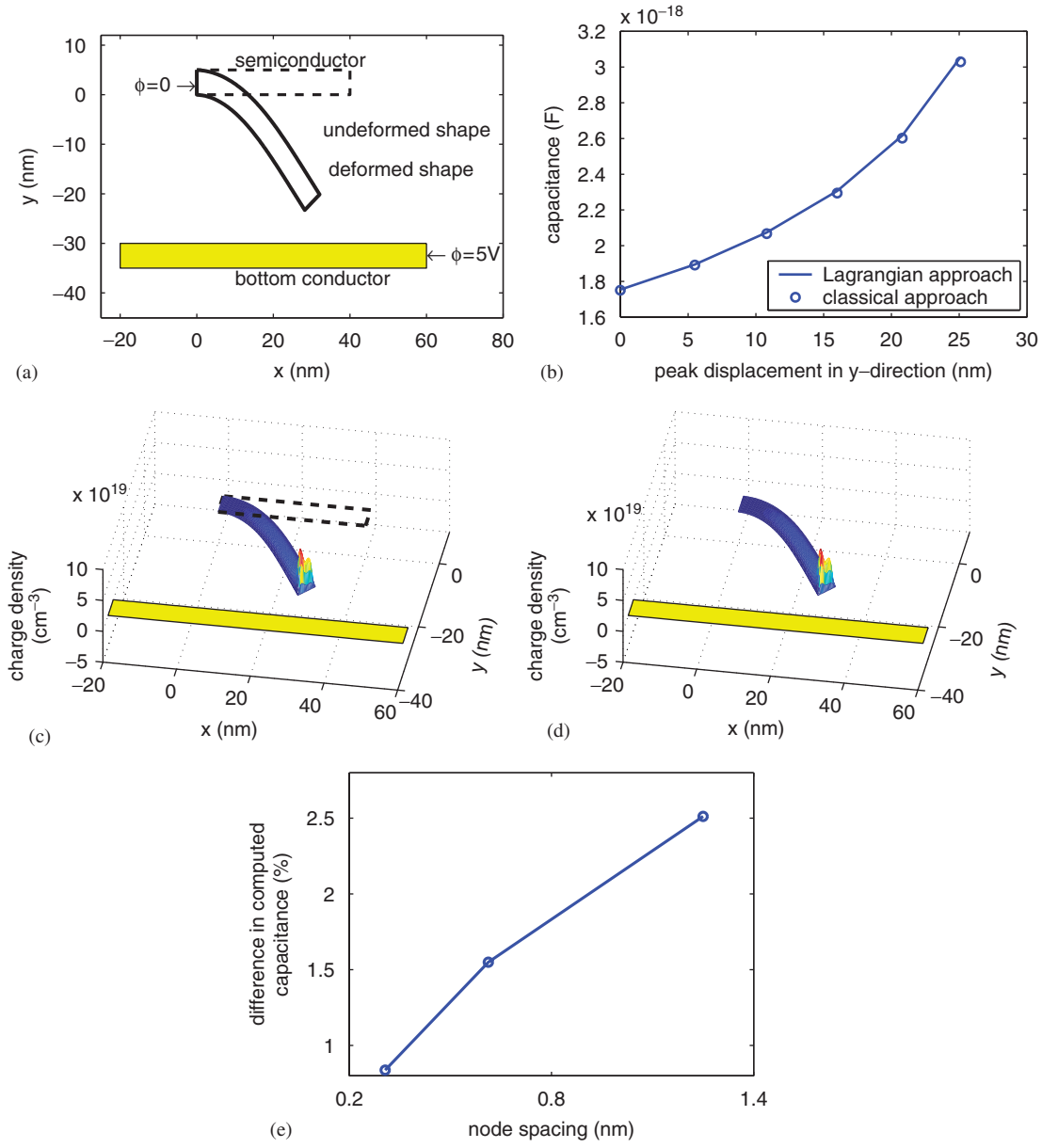

Fig. 7. A cantilever nanoswitch example: (a) the top semiconductor beam is subjected to a large bending deformation; (b) capacitance variation as a function of the peak displacement; (c) charge distribution in the deformed semiconductor beam obtained from the Lagrangian approach; (d) charge distribution in the deformed semiconductor beam obtained from the deformed configuration approach; (e) capacitance difference between the two approaches.

The third example is a nanoswitch subjected to a large deformation. The nanoswitch contains a 40 nm × 5 nm silicon cantilever beam and a 80 nm long bottom conductor, as shown in Fig. 7(a). The initial gap is 30 nm. The beam has an N-type doping density of $10^{15}/cm^3$. The potential at the left end of the beam is specified as 0 V. The applied potential on the bottom conductor is 5 V. The deformation of the cantilever nanoswitch is obtained from a mechanical analysis (see [7] for details). The capacitance variation as the beam deforms is shown in Fig. 7(b). The charge density computed by the Lagrangian approach is shown in Fig. 7(c) and the charge density computed by the deformed configuration approach is shown in Fig. 7(d). The top semiconductor is discretized into 32 × 4, 64 × 8 and 128 × 16 points and the boundary of the structures is discretized into 116, 228 and 452 cells, respectively. The capacitance difference between the two approaches is found to be 2.5% for a discretization of 32 × 4 points and 116 cells. The capacitance difference is larger compared to the second example due to the larger deformation of the beam. When 128 × 16 points and 452 cells are used, the difference between the two approaches reduces to 0.8%.

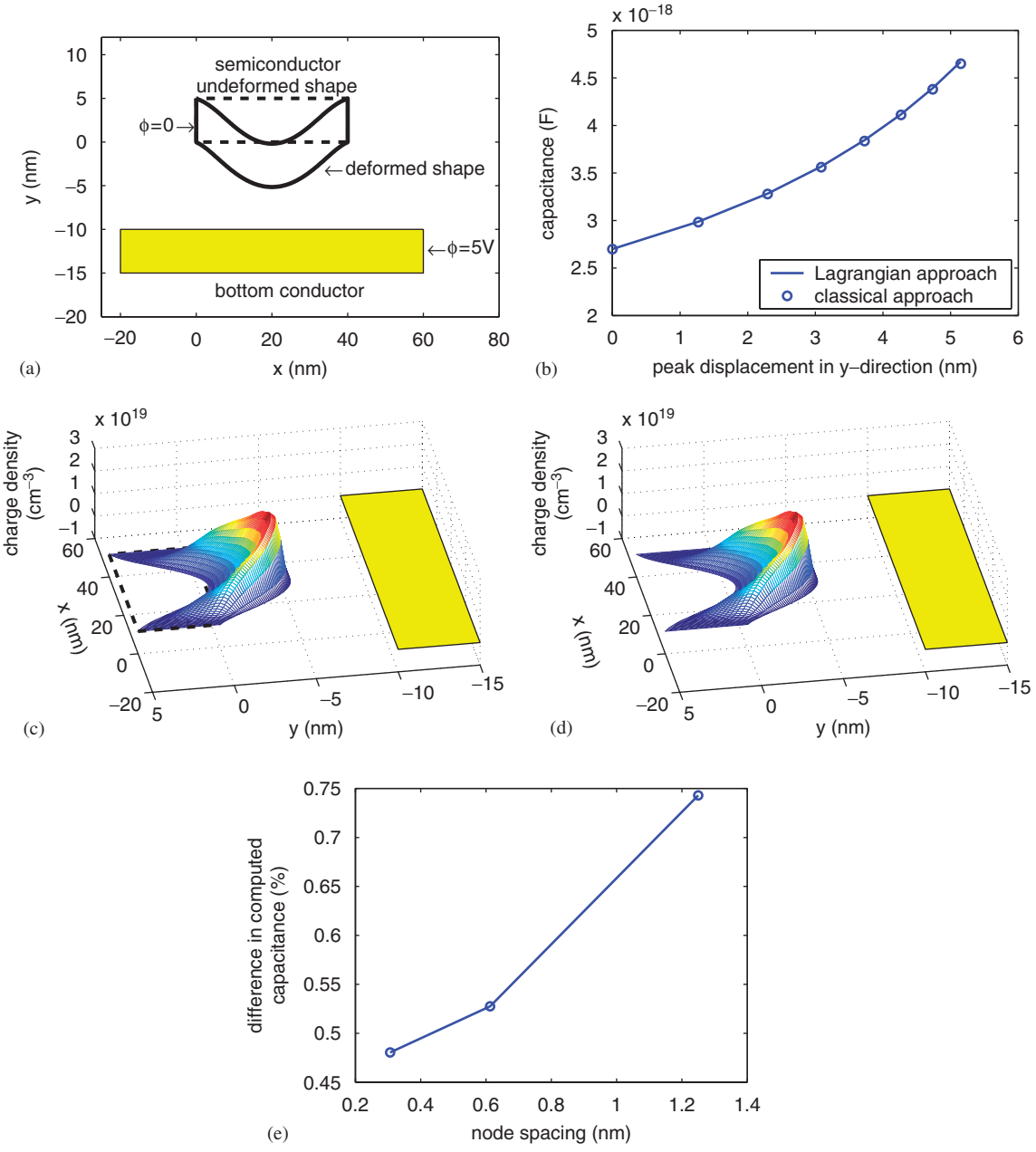

Fig. 8. A fixed–fixed nanoswitch example: (a) the top semiconductor beam is subjected to a bending deformation; (b) capacitance variation as a function of the displacement; (c) charge distribution in the deformed semiconductor beam obtained from the Lagrangian approach; (d) charge distribution in the deformed semiconductor beam obtained from the deformed configuration approach; (e) capacitance difference between the two approaches.

The final example is a fixed–fixed nanoswitch example. As shown in Fig. 8(a), a 40 nm × 5 nm silicon fixed–fixed beam is located above a 80 nm × 5 nm bottom conductor, with an initial gap of 10 nm. The beam has an N-type doping density of $10^{15}/cm^3$. The potential at the two ends of the top beam is specified as 0 V. The applied potential on the bottom conductor is 5 V. The deformation of the fixed-fixed nanoswitch is obtained from a mechanical analysis (see [7] for details). The capacitance variation as the beam deforms is shown in Fig. 8(b). The charge density computed by the Lagrangian approach is shown in Fig. 8(c) and the charge density computed by the deformed configuration approach is shown in Fig. 8(d). The semiconductor beam is discretized into 32 × 4, 64 × 8 and 128 × 16 points and the boundary of the structures is discretized into 116, 228 and 452 cells, respectively. As shown in Fig. 8(e), the capacitance difference between the Lagrangian and the deformed approaches is found to be 0.75% for a discretization of 16 × 4 points with 116 cells and 0.48% for the discretization of 128 × 16 points with 452 cells.

6. Conclusions

In this paper, we have introduced a Lagrangian BIE/Poisson/Schrödinger approach to compute the charge distribution in nanoscale deformable semiconductors. This approach is mathematically equivalent to the deformed configuration BIE/Poisson/Schrödinger approach. However, the Lagrangian approach possesses several advantages: (1) it does not require any update of the geometry of the structures, (2) it eliminates integration error that arises when flat panels are used to approximate curved surfaces and (3) interpolation functions need not be re-computed whenever a structure undergoes a shape change. For these reasons, the Lagrangian approach is more efficient and accurate as it avoids the additional computational cost and the numerical error introduced by updating the geometry. The combination of a Lagrangian approach for quantum mechanical electrostatic analysis with a Lagrangian approach for mechanical analysis can significantly simplify coupled electrical and mechanical analysis of NEMS.

Acknowledgments

This research was supported by the National Science Foundation under Grant no. EEC 0228390. This support is gratefully acknowledged.

References

[1] Roukes ML. Nanoelectromechanical systems. Solid-State Sensor and Actuator Workshop, Hilton Head, 2000. p. 367–76.
[2] Yang YT, Ekinci KL, Huang XMH, Schiavone LM, Roukes ML, Zorman CA, et al. Monocrystalline silicon carbide nanoelectromechanical systems. Appl Phys Lett 2001;78:162–4.
[3] Pescini L, Lorenz H, Blick RH. Mechanical gating of coupled nanoelectromechanical resonators operating at radio frequency. Appl Phys Lett 2003;82(3):352–4.
[4] Tang Z, Xu Y, Li G, Aluru NR. Physical models for coupled electromechanical analysis of silicon NEMS. J Appl Phys 2005;97(11) art. no. 114304.
[5] Aluru NR, White J. An efficient numerical technique for electromechanical simulation of complicated microelectromechanical structures. Sensors Actuators A 1997;58:1–11.
[6] Li G, Aluru NR. A Lagrangian approach to compute electrostatic forces on deformable MEMS. J Microelectromechanical Syst 2002;11(3):245–54.
[7] Li G, Aluru NR. Efficient mixed-domain analysis of electrostatic MEMS. IEEE Trans Comput-Aided Des Integrated Circuits Syst 2003;22(9):1228–42.
[8] Shrivastava V, Aluru NR, Mukherjee S. Numerical analysis of 3D electrostatics of deformable conductors using a Lagrangian approach. Eng Anal Boundary Elem 2004;28(6):583–91.
[9] De SK, Aluru NR. Full-Lagrangian schemes for dynamic analysis of electrostatic MEMS. J Microelectromechanical Syst 2004;13(5):737–58.
[10] Ando T, Fowler A, Stern S. Electronic properties of two-dimensional systems. Rev Mod Phys 1982;54:437–672.
[11] Stern F. Self-consistent results for n-type Si inversion layers. Phys Rev B 1972;5:4891–9.
[12] Pacelli A. Self-consistent solution of the Schrödinger equation in semiconductor devices by implicit iteration. IEEE Trans Electron Devices 1997;44:1169–71.
[13] Li G, Aluru NR. Hybrid techniques for electrostatic analysis of nanoelectromechanical systems. J Appl Phys 2004;96(4):2221–31.
[14] Wang X, Newman JN, White J. Robust algorithms for boundary-element integrals on curved surfaces. Proceedings of the first international conference on modeling and simulation of microsystems, semiconductors, sensors and actuators (MSM 00), 2000. p. 473–6.
[15] Mukherjee S, Bao ZP, Roman M, Aubry N. Nonlinear mechanics of MEMS plates with a total Lagrangian approach. Comput Struct 2005;83(10–11):758–68.
[16] Belytschko T, Krongauz Y, Organ D, Fleming M, Krysl P. Meshless methods: an overview and recent developments. Comput Methods Appl Mech Eng 1996;139:3–47.
[17] Aluru NR, Li G. Finite cloud method: a true meshless technique based on a fixed reproducing kernel approximation. Int J Numer Methods Eng 2001;50(10):2373–410.
[18] Jin X, Li G, Aluru NR. On the equivalence between least-squares and kernel approximation in meshless methods. CMES: Comput Modeling Eng Sci 2001;2(4):447–62.
[19] Jin X, Li G, Aluru NR. Positivity conditions in meshless collocation methods. Comput Methods Appl Methods Eng 2004;193(12–14):1171–202.
[20] Jin X, Li G, Aluru NR. New approximations and collocation schemes in the finite cloud method. Comput Struct 2005;83(17–18):1366–85.
[21] Li G, Aluru NR. Boundary cloud method: a combined scattered point/boundary integral approach for boundary-only analysis. Comput Methods Appl Mech Eng 2002;191(21–22):2337–70.
[22] Li G, Aluru NR. A boundary cloud method with a cloud-by-cloud polynomial basis. Eng Anal Boundary Elem 2003;27(1):57–71.
[23] Mukherjee YX, Mukherjee S. The boundary node method for potential problems. Int J Numer Methods Eng 1997;40:797–815.
[24] Telukunta S, Mukherjee S. An extended boundary node method for modeling normal derivative discontinuities in potential theory across edges and corners. Eng Anal Boundary Elem 2004;28:1099–110.
[25] Tang Z, Zhao H, Li G, Aluru NR. Finite temperature quasicontinuum method for multiscale analysis of silicon nanostructures. Phys Rev B 2006;74(6), art.no. 064110.
[26] Pierret RF. Semiconductor device fundamentals. Reading, MA: Addison-Wesley; 1996.

[27] Rae AIM. Quantum mechanics. Bristol: IOP; 1992.
[28] Kane JH. Boundary element analysis in engineering continuum mechanics. Englewood Cliffs, NJ: Prentice-Hall; 1994.
[29] Jackson JD. Classical electrodynamics. 3rd ed. New York: Wiley; 1999.
[30] Chandrasekharaiah DS, Debnath L. Continuum mechanics. New York: Academic Press; 1994.
[31] Malvern LE. Introduction to the mechanics of continuum medium. Englewood Cliffs, NJ: Prentice-Hall; 1969.
[32] Haugerud BM, Bosworth LA, Belford RE. Elevated-temperature electrical characteristics of mechanically strained Si devices. J Appl Phys 2004;95(5):2792–6.
[33] Nakaharai S, Tezuka T, Sugiyama N, Moriyama Y, Takagi S. Characterization of 7-nm-thick strained Ge-on-insulator layer fabricated by Ge-condensation technique. Appl Phys Lett 2003;83(17):3516–8.
[34] Haug EJ, Choi KK, Komkov V. Design sensitivity analysis of structural systems. New York: Academic Press; 1986.